



# Altered structural connectivity of the motor subnetwork in multiple system atrophy with cerebellar features

Apurva Shah<sup>1</sup> · Shweta Prasad<sup>2</sup> · Bharti Rastogi<sup>1</sup> · Santosh Dash<sup>3</sup> · Jitender Saini<sup>4</sup> · Pramod Kumar Pal<sup>3</sup> · Madhura Ingahalikar<sup>1</sup>

Received: 21 August 2018 / Revised: 10 October 2018 / Accepted: 6 November 2018 / Published online: 14 December 2018

© European Society of Radiology 2018

## Abstract

**Objectives** To investigate the structural connectivity of the motor subnetwork in multiple system atrophy with cerebellar features (MSA-C), a distinct subtype of MSA, characterized by predominant cerebellar symptoms.

**Methods** Twenty-three patients with MSA-C and 25 age- and gender-matched healthy controls were recruited for the study. Disease severity was quantified using the Unified Multiple System Atrophy Rating Scale (UMSARS). Diffusion MRI images were acquired and used to compute the structural connectomes (SCs) using probabilistic fiber tracking. The motor network with 12 brain regions and 26 cerebellar regions was extracted and was compared between the groups using analysis of variance at a global (network-wide), nodal (at each node), and edge (at each connection) levels, and was corrected for multiple comparisons. In addition, the acquired connectivity measures were correlated with duration of illness, total Unified MSA Rating Scale (UMSARS), and the motor component score.

**Results** Significantly lower global network metrics—global density, transitivity, clustering coefficient, and characteristic path length—were observed in MSA-C (corrected  $p < 0.05$ ). Reduced nodal strength was observed in the bilateral ventral diencephalon, the left thalamus, and several cerebellar regions. Network-based statistics revealed significant abnormal edge-wise connectivity in 40 connections (corrected  $p < 0.01$ ), with majority of deficits observed in the cerebellum. Finally, significant negative correlations were observed between UMSARS scores and thalamic and cerebellar connectivity ( $p < 0.05$ ) as well as between duration of illness and cerebellar connectivity.

**Conclusions** Abnormal connectivity of the basal ganglia and cerebellar network may be causally implicated for the motor features observed in MSA-C.

## Key Points

- Structural connectivity of the motor subnetwork was explored in patients with multiple system atrophy with cerebellar features (MSA-C) using probabilistic tractography.
- The motor subnetwork in MSA-C has significant alterations in both basal ganglia and cerebellar connectivity, with a higher extent of abnormality in the cerebellum.
- These findings may be causally implicated for the motor features of cerebellar dysfunction and parkinsonism observed in MSA-C.

---

Apurva Shah and Shweta Prasad have equal contribution.

**Electronic supplementary material** The online version of this article (<https://doi.org/10.1007/s00330-018-5874-4>) contains supplementary material, which is available to authorized users.

---

✉ Pramod Kumar Pal  
palpramod@hotmail.com

✉ Madhura Ingahalikar  
mingahalikar@gmail.com

<sup>1</sup> Symbiosis Center for Medical Image Analysis and Symbiosis Institute of Technology, Symbiosis International University, Lavale, Mulshi, Pune, Maharashtra 412115, India

<sup>2</sup> Department of Clinical Neurosciences and Neurology, National Institute of Mental Health & Neurosciences, Hosur Road, Bangalore, Karnataka 560029, India

<sup>3</sup> Department of Neurology, National Institute of Mental Health & Neurosciences, Hosur Road, Bangalore, Karnataka 560029, India

<sup>4</sup> Department of Neuroimaging & Interventional Radiology, National Institute of Mental Health & Neurosciences, Hosur Road, Bangalore, Karnataka 560029, India

**Keywords** Multiple system atrophy · Connectome · Diffusion tensor imaging · Cerebellum

### Abbreviations

DWI	Diffusion-weighted imaging
FOV	Field of view
GM	Gray matter
HC	Healthy controls
MCP	Middle cerebellar peduncle
MRI	Magnetic resonance imaging
MSA	Multiple system atrophy
MSA-C	Multiple system atrophy with predominant cerebellar features
MSA-P	Multiple system atrophy with predominant parkinsonism
NBS	Network-based statistics
ROI	Region of interest
TE	Echo time
TR	Repetition time
UMSARS	Unified Multiple System Atrophy Rating Scale
WM	White matter

### Introduction

Multiple system atrophy (MSA) is a sporadic, neurodegenerative disorder characterized by a variable combination of progressive autonomic dysfunction, parkinsonism, and cerebellar and pyramidal features [1]. Based on the predominant motor symptoms, MSA can be categorized into MSA with predominant parkinsonism (MSA-P) and MSA with predominant cerebellar dysfunction (MSA-C) [2]. The prevalence of these subtypes shows significant variability in different populations. In Europe and the USA, MSA-P accounts for 58–60% of all cases with MSA [3, 4], whereas in Japan, MSA-C was observed in 83.8% of cases with MSA [5].

MSA-C represents a distinct motor subtype of MSA and is characterized by gait ataxia, limb ataxia, scanning dysarthria, and cerebellar oculomotor dysfunction in addition to autonomic dysfunction and parkinsonism [6]. Neuroimaging plays a critical role in the diagnosis of MSA-C and several studies have reported structural and functional changes associated with the cerebellum in MSA-C [7, 8]. Conventional magnetic resonance imaging (MRI) in MSA-C reveals pontine and cerebellar atrophy, the “hot cross bun sign” observed in 81.4% of patients with MSA-C [9], as well as middle cerebellar peduncle and cerebellar hyperintensities [10]. Volumetric studies have reported reduced striatal, brainstem, and cerebellar volumes [11]. Studies using diffusion-weighted imaging (DWI) in MSA-C have observed increased diffusivity of the pons and middle cerebellar peduncle (MCP), and reduced fractional anisotropy in the MCP, inferior cerebellar peduncle, basis pontis, and internal capsule [12–15].

Hypometabolism of the cerebellum and brainstem has been reported in nuclear imaging studies [16].

Neuroimaging studies investigating the structural connectivity are crucial to understand the interactions between various regions of interest that cannot be ascertained through techniques like voxel-based morphometry. A recent study by Wang et al reported a significant reduction in cerebellar fiber density, and impairment of frontal and occipital white matter connectivity in MSA-C [17]. Lu et al reported altered small-world architecture with reduced cerebellar network strength in MSA-C [18]. However, these studies relied on diffusion images acquired on a 1.5-T MRI and employed deterministic tractography which may be not be sensitive in detecting complete fiber pathways.

This work focuses on the motor features of MSA-C and hypothesizes that patients with MSA-C would demonstrate significantly higher abnormality in the cerebellar network in comparison to the basal ganglia network. In order to confirm this hypothesis, we utilized probabilistic tractography to explore the structural connectivity of the motor subnetwork in MSA-C. This subnetwork comprising the precentral cortex, basal ganglia, thalamus, ventral diencephalon, and cerebellum has been previously utilized in connectivity-based studies in Parkinson’s disease [19, 20].

### Methods

#### Subject recruitment and clinical evaluation

This study included 48 subjects, of which 23 were patients with MSA-C and 25 were age- and gender-matched healthy controls (HC). All patients were recruited from the general neurology outpatient clinic and movement disorder clinic. The diagnosis of MSA was based on the criteria by Gilman et al [2], as per which patients were classified as MSA-C based on the predominant motor symptom at evaluation. Demographic details such as gender, age, age at onset, and duration of illness were recorded. Disease severity was quantified using the Unified Multiple System Atrophy Rating Scale (UMSARS) [21]. This study was approved by the Institutional Ethics Committee. All subjects provided informed consent prior to recruitment.

#### Imaging protocol

All MRI scans were performed in a 3-T Philips Achieva MRI scanner using a 32-channel head coil. 3D T1 images with high resolution were obtained with the following parameters: echo time (TE), 3.7 ms; repetition time (TR), 8.1 ms; field of view (FOV), 256 × 256 × 155 mm; slice thickness, 1 mm; voxel

size,  $1 \times 1 \times 1$  mm; sense factor, 3.5; acquisition matrix,  $256 \times 256$ ; flip angle,  $8^\circ$ ; 165 sagittal slices. DWI was acquired using a single-shot spin-echo, echo-planar sequence in axial sections with the following parameters: TE, 62 ms; TR, 8783 ms; FOV,  $224 \times 224$  mm; voxel size,  $1.75 \times 1.75 \times 2$  mm; diffusion gradient directions, 15;  $b$  value,  $1000 \text{ s/mm}^2$ ; and a single  $b = 0 \text{ s/mm}^2$  image.

## Image analysis

### Image pre-processing

Pre-processing of diffusion MRI data was performed using FSL 5.0.9 (<https://fsl.fmrib.ox.ac.uk>). The initial steps involved correction for motion and distortions induced by eddy current. This was performed using “eddy\_correct” which employs affine transformation of the DWI images to the baseline  $b = 0$  images using FSL [22]. Based on appropriate reorientation,  $b$ -matrices were then adjusted to match the transformed images. Subsequently, brain extraction was performed using the brain extraction tool [23]. Pre-processing of T1 images was performed using Freesurfer 6.0 (<http://surfer.nmr.mgh.harvard.edu>). The steps involved were removal of non-brain tissue, bias correction, and segmentation into gray matter (GM), white matter (WM), and cerebrospinal fluid.

### Creating structural connectomes (Fig. 1)

The first step in obtaining the complete connectome involved defining the nodes. In the present study, obtaining detailed nodes of the cerebellum was important as determining connectivity from various cerebellar nodes was crucial to investigate our hypothesis. To achieve this, two atlases were fused to define the nodes: the Desikan atlas from Freesurfer [24] which accurately delineated the complete brain and the AAL atlas which defined multiple regions of interest (ROIs) within the cerebellum. Spherical registration using Freesurfer [25] was performed to map the Desikan ROIs onto the T1 native space and to obtain accurate GM and WM parcellations (which included the cerebellum). Deformable registration via attribute matching and mutual-saliency weighting (DRAMMS) [26] was employed to match the AAL atlas to the native T1 space, and to transfer the cerebellar parcellations. This relies on multi-scale and multi-orientation Gabor attributes and mutual-saliency in which it assigns higher weights to those voxels which have higher ability of uniqueness.

A boundary between the GM and WM was obtained by dilating the WM mask with a 2-mm radius sphere, obtained from Freesurfer, and then intersecting it with the GM mask. The labels of the Desikan atlas (84 regions) except the cerebellum were then mapped onto this boundary by multiplying the label image with the boundary image. Similarly, the AAL

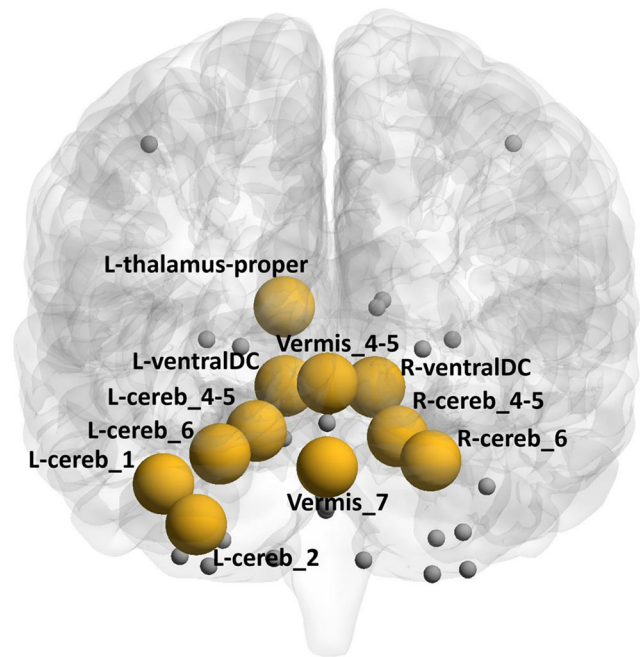


**Fig. 1** Node strength of patients with MSA-C versus healthy controls. Reduced nodal strength was observed in the left thalamus, left ventral diencephalon, right ventral diencephalon, left cerebellum crus 1,2, left cerebellar lobule 4,5, right cerebellar lobule 4,5 left cerebellar lobule 6, right cerebellar lobule 6, vermis 4,5, and vermis 7. Cereb, cerebellum; L, left; R, right; Ventral DC, ventral diencephalon

cerebellum labels (26 regions) were mapped onto the computed boundary and a total of 110 nodes were obtained.

Probabilistic tractography [27] was implemented to track fibers from each node to every other node using the FSL toolbox [22]. In the initial stage, construction of voxel-wise distribution was carried out using a Markov chain Monte Carlo sampling on principle diffusion direction. Probabilistic fiber tracking was then run from each of the computed node boundaries to every other region boundary, by repeatedly sampling from the diffusion distributions at each seed voxel, calculating the streamline such that each sample followed and then using the results to create a distribution of possible tracks weighted by their probability [27]. Fiber tracking was initiated by using the default parameters of 5000 sample streamlines for each voxel and two fibers per voxel in each seed region. Here, a  $110 \times 110$  matrix was created of conditional probability values  $p_{ij}$  between the seed ROI,  $i$ , and the target ROI,  $j$ , given by  $p_{ij} = S_{i \rightarrow j} / S_i$  where  $S_{i \rightarrow j}$  denotes the number of fibers reaching the target region  $j$  from the seed region  $i$  and  $S_i$  is the number of streamlines seeded in  $i$ . The self-connections were represented by zero, while the other connections  $p_{ij} \approx p_{ji}$ , which on averaging provided an undirected weighted connectivity matrix. Finally, based on our hypothesis of differences in the motor subnetwork, we extracted 38 ROIs to create a  $38 \times 38$  subnetwork as shown in Fig. 1. The ROIs selected included the bilateral precentral cortex, basal ganglia, thalamus, ventral diencephalon, and cerebellum.

## Connectome-based statistical analysis

Population analysis was performed only for the above described motor subnetwork of the HC and MSA-C subjects at various levels of granularity: the edge level, the node level (local), and the entire subnetwork level (global). The brain connectivity toolbox [28] was used for computing the standard topological features of the graph and SPSS version 16 was used for performing group-based statistics. The network-based statistic (NBS) toolbox introduced by Zalesky et al [29] was utilized for performing the edge-wise analysis.

### Global measures

Global parameters were used to investigate the differences in the entire motor subnetwork between the two groups. Density, modularity, transitivity, global efficiency, characteristic path length, clustering coefficient, and assortativity coefficient in the motor subnetwork were computed. Definitions of these measures are provided in the [supplementary table](#). Details about these network parameters have been explained elsewhere [28].

### Nodal measures

In order to investigate the differences between the motor subnetwork of MSA-C and HC, several node measures were computed. These included nodal degree, nodal strength, local efficiency, betweenness centrality, and eigenvector centrality. Definitions of these measures are provided in the [supplementary table](#).

## Statistical analyses

### Global and nodal measures

To test our hypothesis, statistical analysis was performed between the two groups for each of the global and nodal measures described earlier. We used a multivariate analysis of covariance model with group as the main factor and age, gender, and normalized cerebellum volumes as covariates. False discovery rate with a threshold of  $q$  value = 0.05 was employed to constraint false positives when performing multiple comparisons in the global network-based and nodal network-based analyses.

### Edge-wise analyses

We performed edge-wise analyses using NBS which is a powerful tool used to identify the alteration in the structural connectivity between pairs of regions of the two groups [29]. We tested for differences between MSA-C and HC for each of the connections of the motor subnetwork with age, gender, and normalized cerebellum volumes as nuisance variables. To correct for multiple comparisons, 10,000 permutations were

applied with a  $t$  value threshold of 2.5 and  $p$  value threshold of 0.01. We performed these statistic tests on both the contrasts, i.e., HC > patients and patients > HC.

### Correlations

The global, nodal, and edge strengths were correlated with the duration of illness, total UMSARS score, and motor component scores. All scores were adjusted for age, gender, and normalized cerebellum volumes by linear regressions and the resulting standard residuals were utilized in correlations. Pearson's  $r$  was computed, and the significance threshold of the correlation was maintained at  $p$  value < 0.05.

## Results

### Demographic and clinical data

Forty-eight subjects were included in this study, of which 23 were MSA-C and 25 were HC. Demographic and clinical details are provided in Table 1. There were no significant differences between MSA-C and HC with respect to the age or gender. The mean age at onset of MSA-C was  $51.41 \pm 6.06$  years and mean duration of illness was  $2.45 \pm 1.18$  years. The total UMSARS (part I + II) score was  $35.31 \pm 17.30$ , and the motor severity (part II) score was  $18.63 \pm 9.27$ . All patients with MSA-C had poor response to levodopa and were on amantadine and vitamin E.

### Global measures

Significant decrease in density (corrected  $p$  value < 0.01), transitivity (corrected  $p$  value < 0.01), characteristic path length (corrected  $p$  value < 0.01), and clustering coefficient

**Table 1** Demographic and clinical features of patients with multiple system atrophy with cerebellar features

	MSA-C	Healthy controls
Gender (M:F)	15:08	19:06
Age (years)	$53.86 \pm 6.15$	$53.52 \pm 8.24$
Age at onset (years)	$51.41 \pm 6.06$	–
Duration of illness	$2.45 \pm 1.18$	–
UMSARS*		
Total score (part I + II)	$35.31 \pm 17.30$	–
Part I score (historical review)	$16.68 \pm 8.29$	–
Part II score (motor examination)	$18.63 \pm 9.27$	–

*F* female, *M* male, *MSA-C* multiple system atrophy with cerebellar features, *UMSARS* Unified Multiple System Atrophy Rating Scale  
\*UMSARS of three subjects was not available



(corrected *p* value < 0.01) was observed in motor subnetwork of patients with MSA-C when compared to HC.

**Nodal measures**

Several regions with significantly reduced nodal strength within the motor subnetwork were observed in patients with MSA-C in comparison to HC (Table 2, Fig. 1). No significant differences were observed in terms of nodal degree, local efficiency, betweenness centrality, and eigenvector centrality.

**Edge-wise analysis**

Edge-wise analysis revealed significantly lower connectivity in patients with MSA-C involving 40 connections of the subnetwork (Table 3, Fig. 2).

**Correlations**

A significant negative correlation was observed between connectivity of the thalamus and total UMSARS scores and UMSARS-II score (Fig. 3). At the edge level, a few connections showed significant correlations with the total UMSARS score, and motor severity score (part II). The connections involved were between the left cerebellum 8 and vermis 7, between the left thalamus and left ventral diencephalon, between the left cerebellum 10 and vermis 4,5, and between the left cerebellum 8 and vermis 7. Duration of illness showed a negative correlation between the vermis 6 and vermis 7. Only one connection from the left cerebellum 4,5 to right cerebellum 4,5 demonstrated a positive correlation with duration of illness.

**Table 2** Regions with reduced nodal strength in patients with multiple system atrophy—cerebellar type

Nodal measures	Nodes	T score	p value	q value
Node strength	Left thalamus proper	18.31	< 0.01	0.018
	Left ventral DC	19.47	< 0.01	0.012
	Right ventral DC	20.53	< 0.01	0.008
	Left verbellum crus 1	31.30	< 0.01	0.000
	Left cerebellum crus 2	24.44	< 0.01	0.002
	Left cerebellum 4,5	35.05	< 0.01	0.000
	Right cerebellum 4,5	24.39	< 0.01	0.002
	Left cerebellum 6	26.02	< 0.01	0.001
	Right cerebellum 6	16.11	< 0.01	0.041
	Vermis 4,5	26.44	< 0.01	0.001
	Vermis7	20.22	< 0.01	0.009

DC diencephalon

**Discussion**

In this study, we focused on exploring the alterations in structural connectivity of the motor subnetwork in MSA-C using probabilistic tractography. The motor subnetwork investigated

**Table 3** T statistics significant edges obtained from edge-wise analysis using network-based statistics

Region	↔	Region	T statistics
Cortex LH precentral	↔	Left thalamus proper	3.75
Cortex LH precentral	↔	Left ventral DC	3.84
Left thalamus proper	↔	Left ventral DC	5.74
Left thalamus proper	↔	Left cerebellum crus 2	3.11
Left ventral DC	↔	Right cerebellum crus 1	2.84
Left ventral DC	↔	Right cerebellum 9	2.8
Left cerebellum crus 1	↔	Left cerebellum crus 2	6.86
Left cerebellum crus 1	↔	Right cerebellum crus 2	2.98
Left cerebellum crus 1	↔	Left cerebellum 6	3.99
Right cerebellum crus 1	↔	Right cerebellum crus 2	3.15
Left cerebellum crus 2	↔	Left cerebellum 7b	3.63
Right cerebellum crus 2	↔	Right cerebellum 7b	3.45
Right cerebellum crus 2	↔	Right cerebellum 8	2.95
Left cerebellum 3	↔	Left cerebellum 4,5	3.83
Right cerebellum 3	↔	Right cerebellum 4,5	4.59
Right cerebellum 3	↔	Vermis 3	3.08
Left cerebellum 4,5	↔	Right cerebellum 4,5	3.13
Left cerebellum 4,5	↔	Left cerebellum 6	4.73
Left cerebellum 4,5	↔	Vermis 4,5	4.82
Right cerebellum 4,5	↔	Right cerebellum 6	3.42
Right cerebellum 4,5	↔	Vermis 4,5	4.00
Left cerebellum 6	↔	Vermis 4,5	3.06
Left cerebellum 6	↔	Vermis 6	3.23
Right cerebellum 6	↔	Vermis 6	4.30
Right cerebellum 6	↔	Vermis 7	4.60
Left cerebellum 8	↔	Left cerebellum 9	3.09
Left cerebellum 8	↔	Vermis 7	3.02
Right cerebellum 8	↔	Right cerebellum 7b	3.3
Right cerebellum 8	↔	Right cerebellum 9	3.00
Right cerebellum 9	↔	Right cerebellum 10	2.93
Left cerebellum 10	↔	Left cerebellum 3	3.83
Left cerebellum 11	↔	Right cerebellum 3	2.91
Left cerebellum 12	↔	Right cerebellum 4,5	3.03
Left cerebellum 13	↔	Left cerebellum 9	5.13
Left cerebellum 14	↔	Vermis 1,2	3.83
Left cerebellum 15	↔	Vermis 4,5	3.7
Vermis 1,2	↔	Vermis 3	3.67
Vermis 1,2	↔	Vermis 7	3.12
Vermis 6	↔	Vermis 4,5	3.74
Vermis 6	↔	Vermis 7	3.45

DC diencephalon, LH left hemisphere

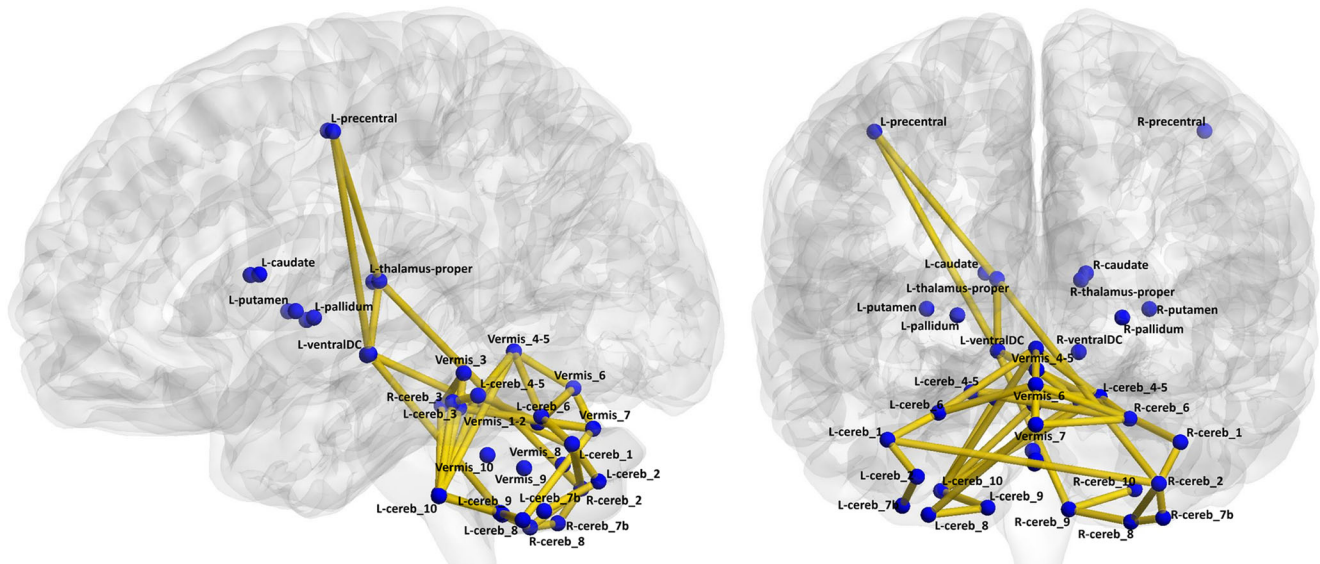


**Fig. 2** Network-based statistics-based edge-wise analysis. Forty abnormal edge-wise connections were observed in patients with MSA-C in comparison to healthy controls. Abnormalities were observed in connections between the cortex and basal ganglia structures, between

comprised of the precentral cortex, basal ganglia, thalamus, and cerebellum. We observed significant widespread abnormalities at global, nodal, and edge levels. Our results provide definitive evidence of damage to connections which may be causally implicated in the motor features of cerebellar dysfunction and parkinsonism observed in MSA-C.

From a functional perspective, the cerebral cortex, basal ganglia, thalamus, and cerebellum may be considered to be highly segregated modules which are part of an integrated network [30]. Within each module, there are nodes with distinct functions and inter and intra modular integration. For instance, the structures of the basal ganglia, i.e., the caudate, putamen,

the basal ganglia and thalamus, between the thalamus and cerebellum, and within the cerebellum, i.e., lobules and the vermis. Cereb, cerebellum; L, left; R, right; Ventral DC, ventral diencephalon

pallidum, and ventral diencephalon, are known to functionally interact with the thalamus and cerebellum, and with each other. Similarly, the cerebellum is also functionally segregated into the cerebello-cerebellum, the spino-cerebellum, and the vestibulo-cerebellum regions [31]. Although each region receives distinct central or peripheral inputs, the outputs converge at similar regions. Furthermore, there is an anatomical overlap between these functionally distinct regions. Hence, abnormalities at any one node, i.e., region within these functional modules, may produce network-wide abnormalities.

We observed significantly abnormal global metrics of the motor subnetwork in the MSA-C group in comparison to HC.

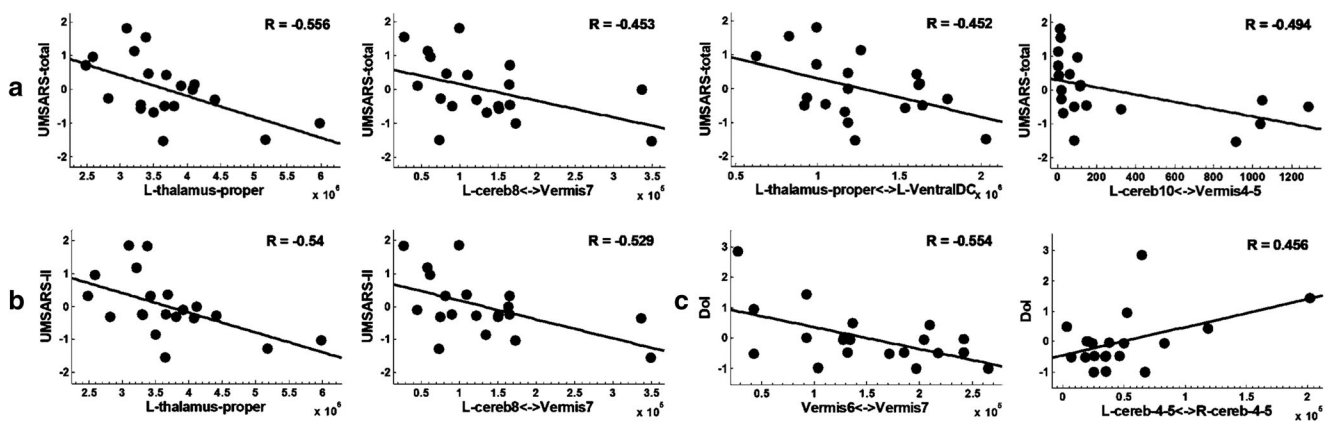


**Fig. 3** Correlation graphs for significant correlations between connectivity metrics and total UMSARS score, motor component score, and duration of illness. Graph (a) shows negative correlations between the total UMSARS score and the left thalamus, and between the total UMSARS score and edge connection between the left cerebellar lobule 8 and vermis 7, between the left thalamus proper and ventral diencephalon, and between the left cerebellar lobule 10 and

vermis 4,5. Graph (b) shows negative correlations between the motor component score and the left thalamus, and between the motor component score and the edge connection between the left cerebellar lobule 8 and vermis 7. Graph (c) shows a negative correlation between the duration of illness and vermis 6 to 7, and positive correlation between duration of illness and left cerebellar lobule 4,5 and right cerebellar lobule 4,5

These findings are suggestive of impairment in the structural segregation, integration, and network resilience of the motor subnetwork in MSA-C. A lower density indicates a reduction in the mean network degree, i.e., a lower number of connections or links to structures in the motor subnetwork. Clustering coefficient and transitivity are measures of functional segregation, and the observed alterations indicate the decreased ability for specialized processing to occur within the motor subnetwork. Impairment in characteristic path length implies a reduction in the structural integration of the motor network. This indicates that the motor subnetwork in MSA-C is unable to effectively combine specialized information from within the subnetwork and from other areas of the brain. These results indicate significant impairment in both the basal ganglia and cerebellum resulting in the symptoms observed in MSA-C. However, these are global measures of the motor subnetwork and do not indicate the extent of abnormality in the each of the structures or connections in the motor subnetwork. This information, which is obtained from nodal measures and edge-wise analysis, is crucial to understand the basis for the predominance of cerebellar symptoms observed in MSA-C.

At a nodal level, we observed significantly reduced nodal strength in several regions, indicating poor connectivity with other nodes. We observed 11 nodes with poor nodal strength (Table 2, Fig. 1), of which 8 were cerebellar nodes. This finding suggests a higher extent of abnormality within the cerebellum in MSA-C.

Edge-wise analysis revealed 40 edges with abnormal connectivity in patients with MSA-C (Table 3, Fig. 2). A higher proportion of abnormal connections involved nodes within the cerebellum and this observation probably substantiates the predominance of cerebellar dysfunction in MSA-C.

The observed negative correlation between the UMSARS scores and thalamus connectivity suggests a definitive involvement of the motor subnetwork in MSA-C. The negative correlations observed between the UMSARS score and the connections between the left cerebellum 8 and vermis 7, between the left thalamus and left ventral diencephalon, between the left cerebellum 10 and vermis 4,5, and between the left cerebellum 8 and vermis 7 imply a definitive role of both cerebellar and extra-cerebellar networks in the disease process. Further, negative correlation of duration of disease with vermis 6 to 7 connection demonstrates that intra-cerebellar connectivity worsens as the disease progresses. Only one correlation demonstrated a positive correlation with duration of illness. This was mainly driven by an outlier, and this correlation became insignificant once the outlier was removed.

Our results observed at a micro-structural level concur with the consistent macro-structural observations of cerebellar atrophy in MSA-C [7, 8, 10, 11]. The results of the present study provide substantial evidence to explain the pattern of motor symptoms observed in MSA-C. Structural connectivity in MSA-C has been previously explored by

Wang et al [17], using deterministic tractography. Although the results reported by the above study are appropriate, the data was acquired using a 1.5-T MRI scanner, which in comparison to 3-T diffusion scans provides very low signal-to-noise ratio and contrast [32]. Furthermore, tract integrity at white matter crossings may not be appropriately measured using deterministic tractography. Seeding of white matter may underestimate small fibers and association fibers and oversample the large fibers [33]. Our approach of probabilistic tractography relied on Monte Carlo-based fiber tracking, which is an improved model of white matter architecture. The fiber tracking in our study was performed directly from the gray matter-white matter boundary of the nodal regions and paths of individual samples were tracked to determine the connectivity between regions.

Our results of impaired structural connectivity contradict the report of higher functional connectivity observed in the cerebellum in MSA-C. Evaluation of resting state functional MRI connectivity in MSA-C revealed higher connectivity in the cerebellar tonsils within the ponto-cerebellar network as compared to subjects with MSA-P and HC [34]. However, as suggested by Roskopf et al [34], it is plausible that the functional hyper-connectivity observed in MSA might be an adaptive response to progressive underlying structural neuro-degeneration.

Even though probabilistic tractography was used in the present study, white matter crossings may not have been ideally measured due to the lower number of gradient directions, 15 in our case [35]. An appropriate sequence with higher number of diffusion gradient directions and higher order models should be employed to overcome this limitation. However, recently, higher order models employed on lower angular resolution diffusion data have also demonstrated potential to delineate the white matter better than the traditional models [36], which corroborates our analysis. Further, acquisition of  $b=0$  image in the opposite phase-encoding direction was not performed, which may be useful in susceptibility-induced distortion correction. Our sample size was small and future studies with a larger sample size and high angular resolution diffusion imaging are necessary to confirm our findings.

## Conclusions

Significant alterations in the structural connectivity of the motor subnetwork at the global, nodal, and edge levels are observed in MSA-C. The higher degree of abnormality observed in inter- and intra-cerebellar connectivity corroborates with the predominant motor symptom of cerebellar dysfunction. Future studies exploring the structural connectivity of non-motor subnetworks are crucial to aid in a better understanding of the overall disease process in MSA-C.

**Funding** This study has received funding by Department of Science and Technology – Science Education and Research Board (DST-SERB) (ECR/2016/000808) who provided partial funding for setting up the computing facility.

### Compliance with ethical standards

**Guarantor** The scientific guarantors of this publication is Dr Pramod Kumar Pal.

**Conflict of interest** The authors of this manuscript declare no relationships with any companies whose products or services may be related to the subject matter of the article.

**Statistics and biometry** No complex statistical methods were necessary for this paper.

**Informed consent** Written informed consent was obtained from all subjects (patients) in this study.

**Ethical approval** Institutional Review Board approval was obtained.

**Study subjects or cohorts overlap** Some study subjects are part of the cohort used in a manuscript that has recently been accepted by European Radiology (EURA-D-18-00499).

### Methodology

- Prospective
- Case-control study
- Performed at one institution

### References

1. Fanciulli A, Wenning GK (2015) Multiple-system atrophy. *N Engl J Med* 372:249–263
2. Gilman S, Wenning GK, Low PA et al (2008) Second consensus statement on the diagnosis of multiple system atrophy. *Neurology* 71:670–676
3. Köllensperger M, Geser F, Ndayisaba JP et al (2010) Presentation, diagnosis, and management of multiple system atrophy in Europe: final analysis of the European multiple system atrophy registry. *Mov Disord* 25:2604–2612
4. May S, Gilman S, Sowell BB et al (2007) Potential outcome measures and trial design issues for multiple system atrophy. *Mov Disord* 22:2371–2377
5. Yabe I, Soma H, Takei A, Fujiki N, Yanagihara T, Sasaki H (2006) MSA-C is the predominant clinical phenotype of MSA in Japan: analysis of 142 patients with probable MSA. *J Neurol Sci* 249:115–121
6. Ciolli L, Krismer F, Nicoletti F, Wenning GK (2014) An update on the cerebellar subtype of multiple system atrophy. *Cerebellum Ataxias* 1:14
7. Chandran V, Stoessl AJ (2014) Imaging in multiple system atrophy. *Neurol Clin Neurosci* 2:178–187
8. Brooks DJ, Seppi K, Neuroimaging Working Group on MSA (2009) Proposed neuroimaging criteria for the diagnosis of multiple system atrophy. *Mov Disord* 24:949–964
9. Watanabe H, Saito Y, Terao S et al (2002) Progression and prognosis in multiple system atrophy: an analysis of 230 Japanese patients. *Brain* 125:1070–1083
10. Schrag A, Kingsley D, Phatouros C et al (1998) Clinical usefulness of magnetic resonance imaging in multiple system atrophy. *J Neurol Neurosurg Psychiatry* 65:65–71
11. Schulz JB, Skalej M, Wedekind D et al (1999) Magnetic resonance imaging-based volumetry differentiates idiopathic Parkinson's syndrome from multiple system atrophy and progressive supranuclear palsy. *Ann Neurol* 45:65–74
12. Shiga K, Yamada K, Yoshikawa K, Mizuno T, Nishimura T, Nakagawa M (2005) Local tissue anisotropy decreases in cerebellopetal fibers and pyramidal tract in multiple system atrophy. *J Neurol* 252:589–596
13. Oishi K, Konishi J, Mori S et al (2009) Reduced fractional anisotropy in early-stage cerebellar variant of multiple system atrophy. *J Neuroimaging* 19:127–131
14. Yang H, Wang X, Liao W, Zhou G, Li L, Ouyang L (2015) Application of diffusion tensor imaging in multiple system atrophy: the involvement of pontine transverse and longitudinal fibers. *Int J Neurosci* 125:18–24
15. Dash SK, Stezin A, Takalkar T et al (2018) Abnormalities of white and grey matter in early multiple system atrophy: comparison of parkinsonian and cerebellar variants. *Eur Radiol*. <https://doi.org/10.1007/s00330-018-5594-9>
16. Gilman S, Markel DS, Koeppe RA et al (1988) Cerebellar and brainstem hypometabolism in olivopontocerebellar atrophy detected with positron emission tomography. *Ann Neurol* 23:223–230
17. Wang PS, Yeh CL, Lu CF, Wu HM, Soong BW, Wu YT (2017) The involvement of supratentorial white matter in multiple system atrophy: a diffusion tensor imaging tractography study. *Acta Neurol Belg* 117:213–220
18. Lu CF, Soong BW, Wu HM, Teng S, Wang PS, Wu YT (2013) Disrupted cerebellar connectivity reduces whole-brain network efficiency in multiple system atrophy. *Mov Disord* 28:362–369
19. Barbagallo G, Caligiuri ME, Arabia G et al (2017) Structural connectivity differences in motor network between tremor-dominant and nontremor Parkinson's disease. *Hum Brain Mapp* 38:4716–4729
20. Lewis MM, Du G, Sen S et al (2011) Differential involvement of striato- and cerebello-thalamo-cortical pathways in tremor- and akinetic/rigid-predominant Parkinson's disease. *Neuroscience* 177:230–239
21. Wenning GK, Tison F, Seppi K et al (2004) Development and validation of the Unified Multiple System Atrophy Rating Scale (UMSARS). *Mov Disord* 19:1391–1402
22. Smith SM, Jenkinson M, Woolrich MW et al (2004) Advances in functional and structural MR image analysis and implementation as FSL. *Neuroimage* 23(Suppl 1):S208–S219
23. Smith SM (2002) Fast robust automated brain extraction. *Hum Brain Mapp* 17:143–155
24. Desikan RS, Segonne F, Fischl B et al (2006) An automated labeling system for subdividing the human cerebral cortex on MRI scans into gyral based regions of interest. *Neuroimage* 31:968–980
25. Fischl B (2012) FreeSurfer. *Neuroimage* 62:774–781
26. Ou Y, Sotiras A, Paragios N, Davatzikos C (2011) DRAMMS: deformable registration via attribute matching and mutual-saliency weighting. *Med Image Anal* 15:622–639
27. Behrens TE, Berg HJ, Jbabdi S, Rushworth MF, Woolrich MW (2007) Probabilistic diffusion tractography with multiple fibre orientations: what can we gain? *Neuroimage* 34:144–155
28. Rubinov M, Sporns O (2010) Complex network measures of brain connectivity: uses and interpretations. *Neuroimage* 52:1059–1069
29. Zalesky A, Fornito A, Bullmore ET (2010) Network-based statistic: identifying differences in brain networks. *Neuroimage* 53:1197–1207
30. Bostan AC, Strick PL (2018) The basal ganglia and the cerebellum: nodes in an integrated network. *Nat Rev Neurosci*. <https://doi.org/10.1038/s41583-018-0002-7>
31. Roosta T, Nazeri A, Sahraian MA, Minagar A (2014) The human cerebellum: a review of physiologic neuroanatomy. *Neurol Clin* 32: 859–869
32. Alexander AL, Lee JE, Wu YC, Field AS (2006) Comparison of diffusion tensor imaging measurements at 3.0 T versus 1.5 T with and without parallel imaging. *Neuroimaging Clin N Am* 16:299–309 xi



33. Bloy L, Ingalhalikar M, Batmanghelich NK, Schultz RT, Roberts TP, Verma R (2012) An integrated framework for high angular resolution diffusion imaging-based investigation of structural connectivity. *Brain Connect* 2:69–79
34. Roskopf J, Gorges M, Müller HP, Pinkhardt EH, Ludolph AC, Kassubek J (2018) Hyperconnective and hypoconnective cortical and subcortical functional networks in multiple system atrophy. *Parkinsonism Relat Disord* 49:75–80
35. Jones DK, Knösche TR, Turner R (2013) White matter integrity, fiber count, and other fallacies: the do's and don'ts of diffusion MRI. *Neuroimage* 73:239–254
36. Toselli B, Tortora D, Severino M et al (2017) Improvement in white matter tract reconstruction with constrained spherical deconvolution and track density mapping in low angular resolution data: a pediatric study and literature review. *Front Pediatr* 5:182